J Geod (2018) 92:609–624
https://doi.org/10.1007/s00190-017-1082-2

ORIGINAL ARTICLE

GNSS satellite transmit power and its impact on orbit determination

Peter Steigenberger[1] · **Steffen Thoelert**[2] · **Oliver Montenbruck**[1]

Received: 28 July 2017 / Accepted: 15 October 2017 / Published online: 11 November 2017

Abstract Antenna thrust is a small acceleration acting on Global Navigation Satellite System satellites caused by the transmission of radio navigation signals. Knowledge about the transmit power and the mass of the satellites is required for the computation of this effect. The actual transmit power can be obtained from measurements with a high-gain antenna and knowledge about the properties of the transmit and receive antennas as well as losses along the propagation path. Transmit power measurements for different types of GPS, GLONASS, Galileo, and BeiDou-2 satellites were taken with a 30-m dish antenna of the German Aerospace Center (DLR) located at its ground station in Weilheim. For GPS, total L-band transmit power levels of 50–240 W were obtained, 20–135 W for GLONASS, 95–265 W for Galileo, and 130–185 W for BeiDou-2. The transmit power differs usually only slightly for individual spacecraft within one satellite block. An exception are the GLONASS-M satellites where six subgroups with different transmit power levels could be identified. Considering the antenna thrust in precise orbit determination of GNSS satellites decreases the orbital radius by 1–27 mm depending on the transmit power, the satellite mass, and the orbital period.

Keywords Antenna thrust · EIRP · GPS · GLONASS · Galileo · BeiDou

✉ Peter Steigenberger
peter.steigenberger@dlr.de

[1] German Space Operations Center (GSOC), Deutsches Zentrum für Luft- und Raumfahrt (DLR), Münchener Straße 20, 82234 Weßling, Germany

[2] Institute of Communications and Navigation (IKN), Deutsches Zentrum für Luft- und Raumfahrt (DLR), Münchener Straße 20, 82234 Weßling, Germany

1 Introduction

Accurate satellite orbits are a prerequisite for most high-precision applications of Global Navigation Satellite Systems (GNSSs). Precise orbit determination of GNSS satellites needs to take into account even subtle accelerations acting on the satellites. The so-called *antenna thrust* is a small acceleration caused by the transmission of navigation signals by GNSS satellites. Eanes et al. (1999) called this effect "Radiation Rocket" nicely explaining the basic principle. As the GNSS transmit antennas usually point to the center of the Earth (Montenbruck et al. 2015a) and transmit their signals continuously at the same power level, a constant acceleration acts in radial direction that results in a different orbital radius at a given orbital period.

The magnitude of this acceleration depends on the transmit power, the mass of the satellite, and the orbit height. Previous studies by Ziebart et al. (2004) and Ziebart et al. (2007) specify an acceleration due to antenna thrust of 0.26 nm/s^2 for the GPS Block IIR satellites. In a more recent study, Rodriguez-Solano et al. (2012) report a similar acceleration and a radial effect of 5 mm for GPS. For the evolving European satellite navigation system Galileo, even larger effects can be expected as these satellites transmit a variety of navigation signals at four different frequencies in the L-band (1–2 GHz) but also have a smaller mass compared to GPS.

The transmit power required for modeling antenna thrust can be obtained with different methods:

1. Preflight ground measurements typically performed before and after the thermal vacuum tests of the satellite.
2. In-flight measurements of the output power of the high-power amplifier onboard the satellite.

3. Link budget calculations based on the specified minimum received power levels.
4. Ground measurements of the received power with a high-gain antenna.

Only limited results of the first two methods are published. Edgar et al. (1998) report preflight power measurements of the navigation payload of the first GPS Block IIR satellite (G043, launched in July 1997). The output power is 50 W for L1 and 11 W for L2 based on laboratory measurements extrapolated to the expected on-orbit operational temperature. Wu (2002) compares two different types of preflight measurements and in-flight measured power values of the first six GPS Block IIR satellites. The L1 measurements range from 29 to 60 W, the L2 measurements from 9 to 22 W.

The third and fourth methods are based on the received power of a GNSS signal on the Earth's surface, which depends on the actual transmit power, the satellite antenna gain pattern, losses along the propagation path, and the receive antenna gain. This link budget will be discussed in more detail in Sect. 2.1. The interface control documents (ICDs) or interface specifications (ISs) of a GNSS (e.g., IS-GPS-200H 2014) usually include information about minimum received power levels of the individual signals. Together with the link budget, a corresponding minimum transmit power at the satellite can be obtained. The GPS transmit power model (IGS 2011) of the International GNSS Service (IGS, Dow et al. 2009) was derived with such an approach. As the actual received power levels were higher than the specified minimum values, empirical scaling factors were applied for the IGS model, see Sect. 2.3.

Another approach is based on measurements of the emitted isotropic radiation power (EIRP) with a high-gain antenna. If the properties of the transmit antenna and the propagation losses are known, the GNSS satellite transmit power can be obtained from the EIRP measurements. As an example for such a high-gain antenna, the 30-m dish antenna used in this study is shown in Fig. 1. It is operated by the German Space Operations Center (GSOC) at its ground station near Weilheim (Bavaria, Germany) and used by DLR's Institute for Communications and Navigation (IKN) for signal analysis of the Global Positioning System (GPS; Hauschild et al. 2012; Thoelert et al. 2012b), the European Galileo and the Chinese BeiDou (Thoelert et al. 2012a), as well as the Indian Regional Navigation Satellite System (IRNSS; Thoelert et al. 2014). Absolute power levels can be obtained from the high-gain antenna measurements after calibration with a well-known reference, e.g., the radio source Cassiopeia A (Baars et al. 1977).

Edgar et al. (1998) provide signal power measurements for the first Block IIR satellite (G043) as well as GPS Block II/IIA satellites from two different high-gain antennas. The Block II/IIA results were mainly obtained with a 18.3-m parabolic antenna located at the Camp Parks Annex Test facility (Pleasanton, California), whereas a 45.7-m antenna of Stanford Research Institute (SRI) International (Menlo Park, California) was used for G043. Block II/IIA L1 power levels at an elevation of 5° reported in Edgar et al. (1998) are 3–4 dB larger than the minimum received power specified in the corresponding GPS ICD (ICD-GPS-200C 2000). Surface power measurements of G043 range from −155 to −151 dBW for L1 and −160 to −156 dBW for L2. L1 and L2 surface power measurements with the SRI antenna have a standard deviation of about 0.1 dB, and the overall accuracy of the measurement system is given with 0.5 dB. Edgar et al. (2002) report surface power measurements of the complete GPS constellation as of 2001 with the SRI antenna. Power levels are 2–4 dB above ICD-GPS-200C (2000) specifications for L1 and 4–6 dB for L2, respectively. No correlation of the power with the satellite age could be found.

Fig. 1 30-m dish antenna of the German Space Operations Center (GSOC) at its ground station near Weilheim

However, no transmit power values of the latest GPS Block IIF generation as well as the other GNSSs GLONASS, Galileo, and BeiDou have been published up to now. This lack of information is the main motivation for the analyses presented in this publication focusing on the determination of GNSS satellite total transmit power. Section 2 discusses the theoretical background of transmit power determination with a high-gain antenna as well as the current IGS GPS transmit power model in more detail. The practical measurement setup with the Weilheim 30-m antenna as well as results for GPS, GLONASS, Galileo, and BeiDou-2 are presented in Sect. 3. Modeling of antenna thrust and its impact on the orbit determination of GNSS satellites are discussed in Sect. 4.

2 Theory

This section introduces the theoretical background on link budget computations, GNSS satellite antenna gain patterns, and the currently employed IGS transmit power model for GPS.

2.1 Link Budget

The link budget provides a relation between the transmitted power at the satellite and the power received by the user. The link budget of a GNSS satellite is given by

$$P_\mathrm{r} = P_\mathrm{s} + G_\mathrm{s} + G_\mathrm{r} - L_\mathrm{pol} - L_0 - L_\mathrm{atm} \tag{1}$$

with

P_r	received power (dBW)
P_s	transmitted power (dBW)
G_s	transmit antenna gain (dB)
G_r	receive antenna gain (dB)
L_pol	polarization mismatch loss (dB)
L_0	free space loss (dB)
L_atm	atmospheric loss (dB)

The transmit antenna gain is composed of the directivity D_s and the gain correction factor $\mathrm{GCF_s}$:

$$G_\mathrm{s} = D_\mathrm{s} + \mathrm{GCF_s}. \tag{2}$$

For the gain of GNSS user receiver antennas, two different antennas are usually considered in link budget computations: a +3 dBi linearly polarized antenna (e.g., ICD-GPS-200C 2000) or a 0 dBi circularly polarized antenna (e.g., IS-GPS-200H 2014; IS-QZSS-L1S-001 2017). The gain of a parabolic antenna is given by

$$G_\mathrm{r} = 10 \cdot \log k \cdot \left(\frac{\pi \cdot D}{\lambda}\right)^2 \tag{3}$$

with the efficiency factor k and the diameter of the antenna D (Seybold 2005). The gain of the Weilheim 30-m antenna in the L-band with wavelengths $\lambda \approx$ 19 to 25 cm is about 50 dB.

The polarization mismatch loss depends on the axial ratio of the transmit and receive antenna (Schrank 1983). The axial ratio denotes the ratio of the electromagnetic field strength along the major and minor axis of the polarization ellipse. It amounts to 0 dB for a perfectly circular polarization, while nonzero values indicate an elliptic polarization (Visser 2012). Axial ratios of different GNSS transmit antennas are given in Table 1. For a 0.5 dB axial ratio of typical high-gain antennas (Wu 2002), the polarization mismatch loss amounts to roughly 0.03 dB. The total polarization mismatch loss of a high-gain antenna and the GNSS transmit antennas listed in Table 1 for a maximum mismatch angle of 90° varies between 0.01 dB for E1 of the Galileo In-Orbit Validation (IOV) satellites and 0.19 dB for L2 of the old GPS Block I antenna. The maximum value of currently active satellites is 0.07 dB for the low band of Galileo IOV, which can be neglected.

For GNSS receiver antennas, axial ratios at 5° elevation between 1.6 dB for GPS L1 and 6.0 dB for GLONASS L2 are given in NovAtel Inc. (2006) resulting in polarization mismatch losses between 0.1 and 1.1 dB. Commonly used polarization mismatch loss values w.r.t. a linearly polarized receiver antenna for link budget calculations are 3.7 dB (Edgar et al. 1998) or 4.0–4.1 dB (Spence 2010) where 3.0 dB are attributed to the reception of a circularly polarized signal with a linearly polarized antenna.

The free space loss L_0 in dB is given by Ghasemi et al. (2012) as

$$L_0 = 20 \cdot \log \frac{\lambda}{4\pi d} \tag{4}$$

for a distance d between satellite and receiver antenna. The free space loss is the largest contribution to the link budget and varies for GPS between 184.5 dB for L1 at 5° elevation and 180.0 dB for L5 in zenith direction.

The atmospheric loss L_atm is caused by gas absorption primarily due to oxygen as well as attenuation due to rain, snow, fog, and clouds. The gaseous absorption contributes the largest portion for L-band frequencies. ITU-R (2013a) describes a ray-tracing algorithm to compute the attenuation based on a reference standard atmosphere (ITU-R 2013c).

Table 1 Axial ratios of GNSS transmit antennas. High band refers to L1/E1, low band to L2/L5/E5/E6

GNSS	Block	Axial ratio (dB)		Reference
		High band	Low band	
GPS	I	1.2	3.2	Czopek and Shollenberger (1993)
	II	0.8	2.0	Czopek and Shollenberger (1993)
	IIR	0.95	0.85–0.95	Wu (2002)
GAL	IOV	0.5	1.7	Montesano et al. (2007)
	FOC	< 0.7	< 0.6	Valle et al. (2006)

The zenith attenuation is 0.03 dB and increases to 0.4 dB for an elevation of $\varepsilon = 5°$. Spilker Jr. (1996) gives an approximation based on a zenith attenuation of 0.035 dB and a simple uniform spherical shell model of the atmosphere:

$$L_{\mathrm{atm}} = 0.07 \cdot \frac{1 + \frac{a}{2}}{\sin\varepsilon + \sqrt{\sin^2\varepsilon + 2a + a^2}} \tag{5}$$

with

$$a = \frac{H_{\mathrm{m}}}{R_{\mathrm{e}}} \tag{6}$$

and the equivalent height for oxygen $H_{\mathrm{m}} = 6$ km and the Earth radius R_{e}. Differences w.r.t. the ITU model are below 0.016 dB at 5° elevation. Therefore, this approximation will be used in the following.

Further atmospheric effects are negligible for L-band frequencies:

- Attenuation due to rain (ITU-R 2005) is $<$ 0.034 dB for L1 even for an extreme rain rate of 100 mm/h. For a typical heavy rain (25 mm/h), the attenuation is $<$ 0.018 dB.
- Attenuation due to fog is $\ll$ 0.012 dB. This is the attenuation for 10 GHz as the ITU-R (2013b) model is not valid for smaller frequencies.
- Irsigler et al. (2004) give an attenuation due to clouds of $<$ 0.1 dB for L-band frequencies.

The attenuations for rain and fog refer to an elevation of 5° at Weilheim; typical/extreme meteorological values are taken from Mölders and Kramm (2014).

2.2 Transmit antenna gain pattern

The gain pattern of a GNSS transmit antenna is usually designed in such a way that the changes in free space loss due to the varying distance between satellite and receiver are at least partly compensated by the pattern (Ajioka and Harry 1970). For GPS orbit height, this variation is 1.9 dB. The GPS Block I gain pattern for the L1 band is given in Czopek and Shollenberger (1993). However, as the last satellite of this type was decommissioned in 1996, Block I measurements could not be considered in this study. The L1 gain pattern of the GPS II/IIA satellites as given in Spence (2010) is illustrated in Fig. 2. It shows a peak value of about 15 dB at a nadir angle of 10° to compensate the higher free space losses at low elevations, i.e., higher nadir angles.

For the GPS Block IIR satellites, two different subgroups have to be distinguished according to their space vehicle number (SVN): the Block IIR-A satellites (SVN 41, 43–46, 51, 54, 56) with a legacy antenna panel and the Block IIR-B satellites (SVN 47, 59–61) with an improved antenna panel

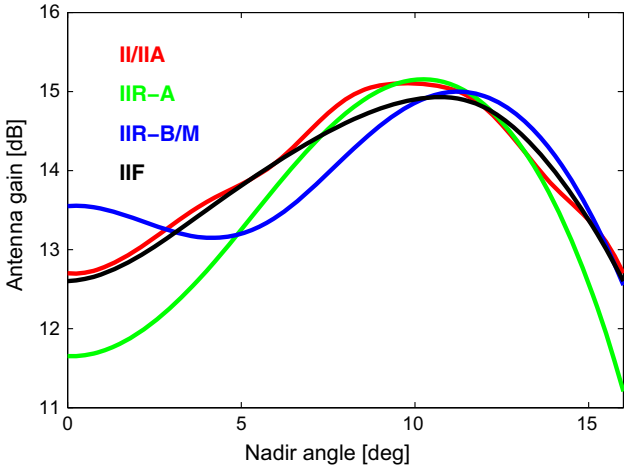

Fig. 2 GPS L1 transmit antenna gain pattern for Block II/IIA, IIR-A, IIR-B/IIR-M, and IIF satellites. For Block IIR-A and IIR-B/IIR-M, mean values of the corresponding satellites as computed from averages of positive and negative nadir angles as well as the different azimuth angles are shown, respectively

that is also used for the Block IIR-M satellites (Marquis and Reigh 2015). Satellite-specific azimuth- and nadir-dependent directivity patterns of the GPS Block IIR and IIR-M satellites for L1 and L2 are given in Marquis (2014); the corresponding GCFs to obtain the gain pattern (see Eq. 2) are listed in Marquis (2016). Please note, though, that a different GCF sign convention has previously been used in Marquis (2015). The gain patterns of the IIR-A and IIR-B/IIR-M satellites differ significantly as illustrated in Fig. 2 for L1. The improved antenna panel provides a higher gain for nadir angles below 3° and above 12° with a lower gain in between.

Fisher and Ghasemi (1999) give a GPS Block IIF L1 gain pattern obtained from measurements of an engineering model of the antenna unit. The pattern is very similar to Block II/IIA as both generations of satellites are assembled by the same manufacturer. However, no L2 and L5 gain pattern are available. In the following, the Block IIF L1 gain pattern of Spence (2010) will be used that differs from the one of Fisher and Ghasemi (1999) by up to 1.5 dB.

The gain pattern of an engineering model of the Galileo IOV antenna for the high band (E1) and the low band (E5/E6) is given in Montesano et al. (2007) and illustrated in Fig. 3. The Galileo Full Operational Capability (FOC) satellites utilize the same basic antenna type as GIOVE-A. Valle et al. (2006) present relative gain measurements of a prototype antenna and simulations for an optimized design that was finally used for GIOVE-A. Compared to GPS (Fig. 2), the Galileo antenna gain patterns (Fig. 3) provide a roughly 1.5 dB higher gain for nadir angles up to 10°.

Due to their significantly different orbit heights, BeiDou-2 satellites in geostationary (GEO) and inclined geosynchronous orbit (IGSO) have a different antenna design

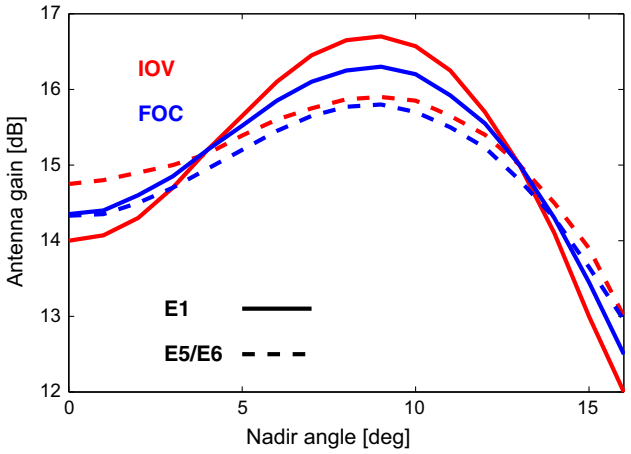

Fig. 3 Galileo transmit antenna gain pattern for in-orbit validation (IOV) and full operational capability (FOC) satellites

than those in medium Earth orbit (MEO). Gain patterns for B1 and B2 of both satellite groups are given in Chang et al. (2015). Due to the lack of a dedicated pattern for B3, the B2 pattern is also used for B3 in the present study. For GLONASS, no gain patterns are publicly available. Therefore, a mean antenna gain of 14 dB for L1 and 13 dB for L2 and L3 is assumed, based on typical values of the other GNSS. The QZS-1 L1 gain pattern is published in Noda et al. (2010), but no measurements of this satellite are possible from Weilheim due to the low elevation.

2.3 Current IGS Model

The GPS transmit power model currently used by the IGS (IGS 2011) is based on the minimum received radio frequency (RF) power as specified in IS-GPS-200E (2010), IS-GPS-705A (2010), and IS-GPS-800A (2010) for a 3 dBi linearly polarized receive antenna and an elevation angle of $\varepsilon > 5°$. For the military M-code, the document specifying the minimum received RF power (IS-GPS-700) is not publicly available. Barker et al. (2000) give a value of -158.0 dBW for L1 and L2 that is used in the IGS model although recent publications indicate a lower transmit power at L2 (Marquis 2016). L1 transmit antenna gain patterns based on measured and calibrated data (Spence 2010) are used for Block IIA, IIR-M, and IIF satellites for the L1 *and* L2 band. For the L5 band of the Block IIF satellites, a predicted gain pattern is used (Spence 2010). An atmospheric loss of 0.5 dB and a polarization mismatch loss of 4.0 dB are applied. To account for the actually higher transmit power reported by Edgar et al. (2002), empirical scaling factors of 3 dB for L1 and 5 dB for L2 are used. Due to a lack of measurements for L5, a scaling factor of 3 dB is applied. The resulting transmit power model of the IGS is listed in Table 2. For the second IGS reprocessing campaign (Rebischung et al. 2016a), an empirical value of 100 W was used for GLONASS to avoid scale inconsistencies between GPS and GLONASS.

Table 2 GPS transmit power values currently used within the IGS (IGS 2011)

GPS block	Power (W)
IIA	76
IIR	85
IIR-M	198
IIF	249

However, the scaling factors mentioned above are too large by 1.5 dB as the measured differences w.r.t. ICD specifications given by Edgar et al. (2002) refer to ICD-GPS-200C (2000), whereas the link budget in Spence (2010) is based on IS-GPS-200E (2010). Major differences between these ICD versions are a reduced and more realistic assumption for the atmospheric loss (0.5 dB instead of 2.0 dB) and an increased minimum received power specification (by 1.5 dB). Therefore, the IGS model values are expected to be too large by about 40%.

3 Measuring GNSS Satellite Transmit Power

A general overview of the setup for measuring EIRP with the Weilheim high-gain antenna is given in Fig. 4. GNSS signals are received in an L-band feed covering a frequency range of 1.1–1.7 GHz with best gain in the E1/L1 and E5a/L5 sub-bands. Even though the feed provides also partial S-band coverage, the gain in this frequency range is notably reduced and exhibits pronounced variations. In the absence of a reliable S-band calibration, this work is confined to L-band navigation signals exclusively. The feed offers dedicated couplers for various types of polarization and has been configured for right-hand circular polarization (RHCP) signals in the present application. After coupling from the feed, the signals are passed to two cascaded stage low-noise amplifiers (LNAs) with intermediate band-pass filters and a total gain of +70 dB. Following the amplification, the signals are passed to a vector signal analyzer (VSA) for downconversion, online spectrum analysis, and recording of raw in-phase and quadrature (I/Q) components. The VSA covers a bandwidth of 120 MHz and offers a sampling frequency of about 150 MHz. For internal calibration, a complementary signal generator is available that can inject calibration signals either before or after the amplification stage. Detailed information on the overall setup is provided in Thoelert et al. (2013).

For calibration of the total system gain, measurements of an extragalactic radio source (typically Cassiopeia A and Cygnus A) are taken on a semi-annual basis and compared with predicted flux data for the period of interest based on the absolute flux measurements in Baars et al. (1977).

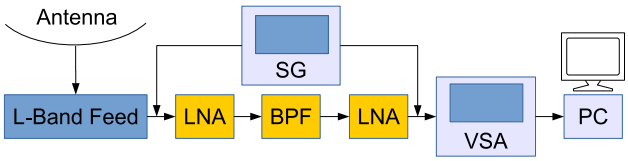

Fig. 4 Schematic overview of the measurement setup at the Weilheim high-gain antenna. LNA: low-noise amplifier, BPF: band-pass filters, VSA: vector signal analyzer, *SG* signal generator, *PC* data system for storage and analysis

Based on a time series of I/Q vectors recorded within the VSA over a representative period of one to a few milliseconds, the received signal spectrum is obtained with a user-selectable resolution and converted to absolute power spectral density using the total gain determined as part of the overall system calibration. Subsequently, an integral over the desired signal band is performed to obtain the total received power within each band and converted to the EIRP using the known distance of the GNSS satellite. Since no atmospheric losses are taken into account in this process, these contributions will later be considered separately in the transmit power computation. Based on the known satellite-station geometry, the station elevation and satellite boresight angles at the measurement epoch are obtained and associated with the measured EIRP. To obtain the EIRP over a wider range of boresight angles with adequate resolution, measurements are typically taken over the full visibility period (rise to set) of a GNSS satellite at representative intervals of about 5 min. Measurements taken on different days evidence a day-to-day repeatability of better than 0.2 dB.

It may be noted that no detailed knowledge of the signal structure is required for the EIRP measurements. By evaluating the power over the full signal band, contributions of all modulated signals (including both open and encrypted signals) are considered in the overall EIRP. The same applies to interplex modulation products (Rebeyrol et al. 2006) of various modernized signals (e.g., GPS C/A + P(Y) + M-code, or Galileo E1 open service and public regulated service signals) that contribute to the total power but cannot be tracked by a GNSS receiver.

3.1 Parameter estimation

EIRP measurements collected with the 30-m antenna are corrected for free space loss (Eq. 4) and atmospheric loss (Eq. 5). These corrected observations are used in a least squares adjustment to solve for the offset w.r.t. the corresponding gain pattern interpolated to the nadir angle of the observations. The observation equation obtained from the link budget (Eq. 1) reads as

$$P_\mathrm{r}(\varepsilon) = P_\mathrm{s} + G_\mathrm{s}(\theta) - L_0(\mathbf{x}^\mathrm{s}, \mathbf{x}_\mathrm{r}) - L_\mathrm{atm}(\varepsilon) \tag{7}$$

with the position of the satellite $\mathbf{x}^\mathrm{s}$ and the receive antenna $\mathbf{x}_\mathrm{r}$. The relation between elevation ε at the receive antenna and the nadir angle θ at the transmit antenna is given by

$$\sin\theta = \sin\left(\varepsilon + \frac{\pi}{2}\right) \cdot \frac{R_\mathrm{e}}{R^\mathrm{s}} \tag{8}$$

with the mean radius of the Earth R_e and the mean orbital radius of the GNSS satellite R^s. EIRP measurements below 4° elevation are not considered due to increased noise.

Figure 5 shows as an example the EIRP measurements of the Galileo satellite E209. The measured EIRP variation with boresight angle closely matches the shape of published gain patterns for E1 and E6. Only minor deviations of up to ± 0.3 dB are visible for E5. The estimated transmit powers are 20.7, 19.1, and 18.1 dBW for the E1, E6, and E5 frequency bands, respectively. The corresponding values in Watt are 119, 81, and 65 W. The formal errors of the least squares adjustment are 0.1 dBW for E1 and E6 and 0.2 dBW for E5. The slightly higher formal errors for E5 are caused by a small difference between the shape of the transmit antenna gain pattern and the shape of the measured EIRP variation with boresight angle as can be seen in the right subplot of Fig. 5.

3.2 Results

The subsequent discussion covers the global navigation systems GPS, GLONASS, Galileo, and BeiDou-2. Individual satellites are identified by their SVN, where the first character (G/R/E/C) identifies the navigation system. BeiDou-2 GEO had to be excluded from our analysis due to their unfavorable and static viewing geometry that does not allow for a proper averaging of gain pattern uncertainties over a wider range of boresight angles. Likewise, the first satellite (J001) of the Japanese Quasi-Zenith Satellite System (QZSS) is not considered as it is only visible at very low elevations at Weilheim. Therefore, the transmit power of 244 W published in Kogure et al. (2017) will be used in Sect. 4. The Indian Regional Navigation Satellite System (IRNSS) could not be covered by the analysis due to the current lack of fully calibrated S-band power measurements. Due to limited measurement capabilities, not all satellites of each constellation are observed but only representative satellites of each Block.

GPS For a long time, Block II/IIA satellites made up the majority of the GPS constellation. The last Block IIA satellite was decommissioned in January 2016. GPS Block IIR satellites transmit the same set of signals as the II/IIA satellites, namely the C/A-code on L1 and the P-code on L1 and L2. For the modernized Block IIR-M satellites, the military M-code was added on L1 and L2 as well as the civil L2C signal. The Block IIF satellites have an additional transmission

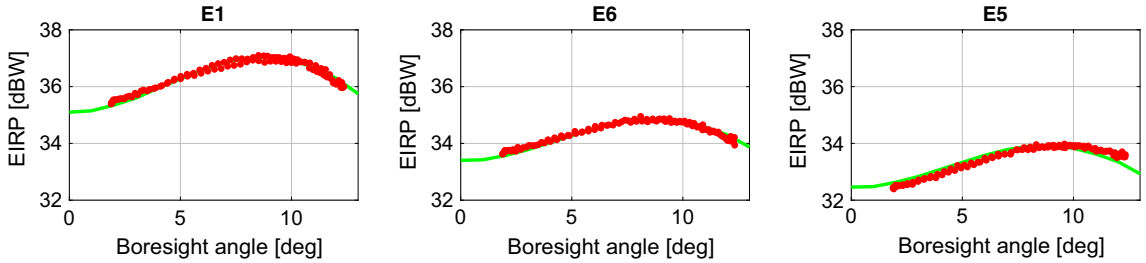

Fig. 5 EIRP measurements of Galileo E209 in the E1, E6, and E5 frequency band (red dots). The green line represents the transmit antenna gain pattern shifted by the estimated transmit power

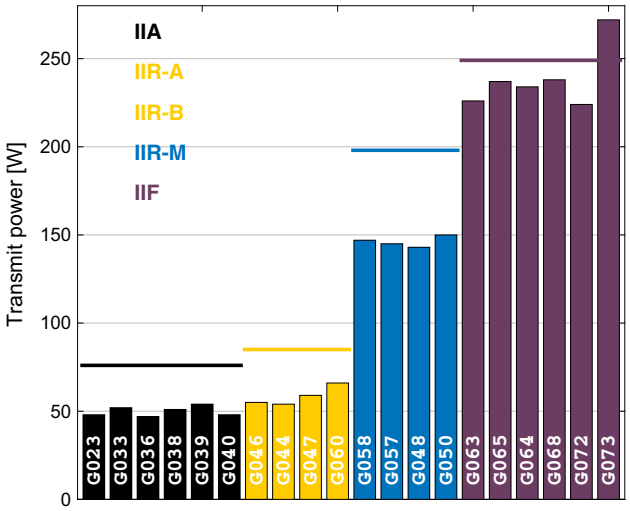

Fig. 6 Total transmit power of different blocks of GPS satellites. The solid lines represent the IGS model as given in Table 2

capability in the L5 band. Within the IGS, two further subgroups of Block IIR satellites are traditionally distinguished due to their different antenna phase center offsets and variations: Block IIR-A with a legacy antenna panel and Block IIR-B with an improved antenna panel that is also used for the Block IIR-M satellites. The two antenna panels have significantly different gain patterns, see Fig. 2, but Block IIR-A and IIR-B satellites are found to exhibit similar transmit power levels.

The different signal transmission capabilities are also reflected in the total GPS transmit power plotted in Fig. 6. Block IIA and IIR satellites have a similar transmit power of about 50 and 60 W, respectively. With values of 143 to 150 W, the transmit power of the IIR-M satellites is almost a factor of three higher. The total power of the Block IIF satellites is mostly between 224 and 238 W; only G073 shows a slightly higher power of 272 W.

The solid lines in Fig. 6 represent the values of the current IGS model as discussed in Sect. 2.3. As expected, the IGS values are too high for Block IIA, IIR, and IIR-M. For Block IIF, the discrepancies are smaller but this might be related to the empirical scaling factor for L5 that is not based on measurements and results in an L5 transmit power of the IGS model that is smaller by a factor of about two compared to the measured power.

According to the Notice Advisory to Navstar Users (NANU) 2011026,[1] M-code transmission of G062 stopped in 2011. NANU 2012035 mentions tests in order to restore the M-code signal of G062, and high-gain antenna measurements of October 2016 confirm the transmission of the M-code signal. However, it is not clear when the M-code transmission started. In February 2017, the transmit power of the L1C/A signal on the Block IIR-M satellites was increased for test purposes (Steigenberger et al. 2017), but the total transmit power stayed constant.

GLONASS The first-generation GLONASS satellites are not considered here as the last satellite of this type was decommissioned in 2010. The current GLONASS constellation is mainly composed of GLONASS-M satellites transmitting FDMA (frequency-division multiple access) C/A- and P-code signals on L1 and L2. The GLONASS-M+ as well -K1 satellites have additional CDMA (code-division multiple access) signals on the L3 frequency. The first GLONASS-K1 satellite (R801) has a separate antenna for the L3 signal (Montenbruck et al. 2015a), whereas later K1 satellites (currently only R802) as well as the GLONASS-M+ satellites transmit all signals via the same antenna.

For GLONASS-M, three different groups of transmit power levels on L1 and L2 could be identified, see Fig. 7:

- L1 high power (L1H): 50–68 W
- L1 medium power (L1M): 38–39 W
- L1 low power (L1L): 17–21 W
- L2 high power (L2H): 19–26 W
- L2 medium power (L2M): 6–7 W
- L2 low power (L2L): 1 W

Based on these transmit power levels, six subgroups of GLONASS-M satellites were formed

[1] Available at https://www.navcen.uscg.gov/.

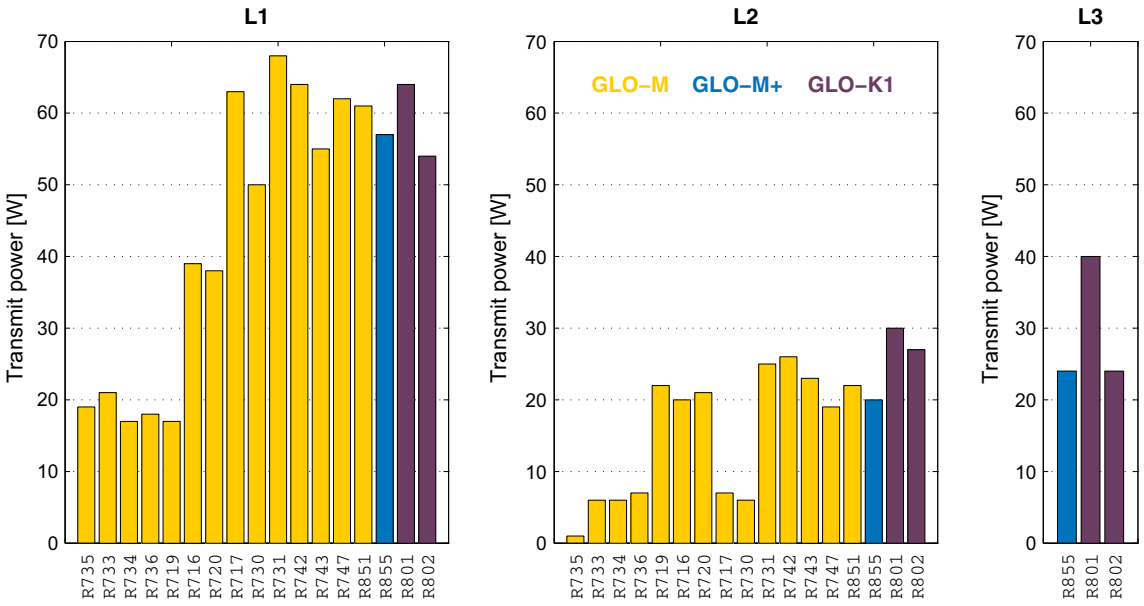

Fig. 7 Band-specific transmit power of GLONASS satellites

- L1L/L2L: R735 launched in 2010
- L1L/L2M: five satellites launched between 2006 and 2010
- L1L/L2H: R719 launched in 2007
- L1M/L2H: two satellites launched in 2006/2007
- L1H/L2L: three satellites launched in 2006, 2009, 2010
- L1H/L2H: all newer satellites launched after 2010 plus R731

The classification of individual GLONASS-M satellites is given in Table 3. Spacecraft of the current GLONASS constellation not covered by high-gain antenna measurements have been assigned to individual groups based on analysis of the carrier-to-noise density ratios (C/N_0) of several GLONASS-capable receivers of the multi-GNSS tracking network of the IGS. R735 launched in 2010 has an extremely low L2 transmit power: It shows a 5 dBW lower EIRP in L2 measurements of April 2017 compared to the L2M group. As no older high-gain antenna measurements are available, C/N_0 time series of R735 have been analyzed. A sudden C/N_0 decrease of about 6 dB-Hz could be identified on February 2, 2016, as illustrated in Fig. 8 for the station Rio Grande (RGDG) in Argentina. The reason for this power loss is unknown; it might be related to a failure of a dedicated part of the transmission chain. As no measurements are available for GLONASS-M spacecraft retired from the current constellation, an average default value of 50 W is recommended for these satellites.

The GLONASS-M+ and the -K1 satellites show an L1 power level that is similar to the L1H group. For L2, the GLONASS-K1 satellites have a higher power of about 30 W as compared to 20 W of GLONASS-M+. The L3 power of

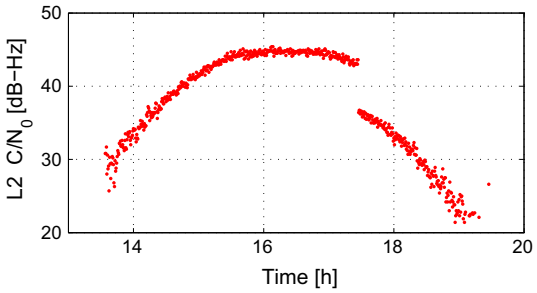

Fig. 8 L2 carrier-to-noise density ratio (C/N_0) time series of GLONASS R735 tracked by the Argentinean station Rio Grande (RGDG) on February 2, 2016. A sudden power loss of about 6 dB can be seen at 17:27 UTC

24 W is the same for the GLONASS-M+ satellite R855 and the GLONASS-K1 satellite R802. At a value of 40 W, the L3 power of the first GLONASS-K1 satellite R801 (which uses a separate L3 antenna) is significantly higher than that of the other L3-capable spacecraft.

Galileo The total transmit power of most Galileo IOV and FOC satellites is shown in Fig. 9. Three different groups of transmit power levels have to be considered for the Galileo IOV satellites. Before May 2014, all four IOV satellites had a transmit power of about 150 W. This measured transmit power is in accord with the power handling capability of the IOV transmit antenna: 103 W for E5 + E6 and 75 W for E1 (Montesano et al. 2007).

On May 27, 2014, around 12:00 UTC, the IOV satellite E104 experienced a sudden power loss followed by a permanent failure of the E5 and E6 transmission capability. As a consequence, the transmit power of all IOV satellites was

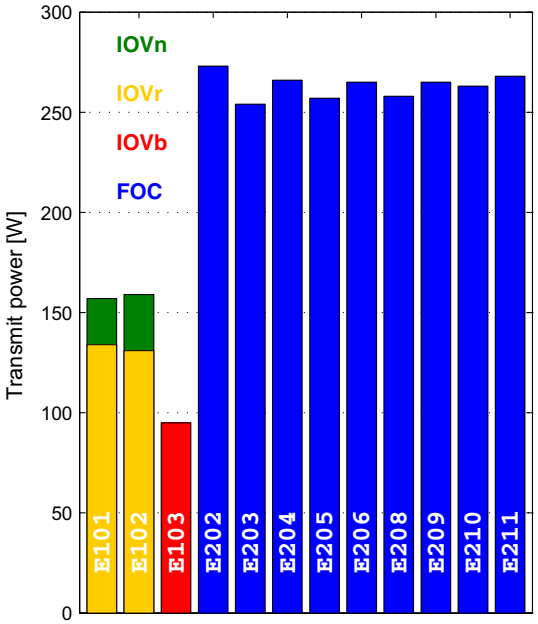

Fig. 9 Total transmit power of Galileo In-Orbit Validation (IOV) and Full Operational Capability (FOC) satellites. IOVn: nominal transmit power; IOVr: reduced transmit power; IOVb: temporary back-off

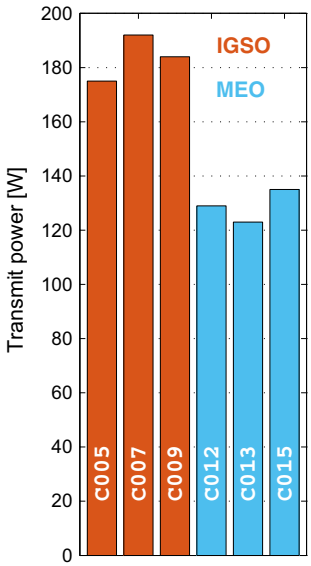

Fig. 10 Total transmit power of BeiDou-2 inclined geosynchronous orbit (IGSO) and medium Earth orbit (MEO) satellites

lowered by 1.5 dB (Steigenberger and Montenbruck 2016). As of summer 2017, there are two different groups of transmit power levels for the three operational Galileo IOV satellites: Galileo E101 and E102 have a transmit power of 134 and 131 W, respectively. Falcone (2016) reports the status "all bands aligned" for these satellites. However, Galileo E103 has still a reduced transmit power of 95 W with the status "all bands in temporary back-off". The transmit power of the FOC satellites is significantly higher compared to IOV and ranges from 254 to 273 W.

BeiDou-2 The transmit power of BeiDou-2 amounts to 175 to 192 W for the IGSO satellites, and 123 to 135 W for the MEO satellites, see Fig. 10. The power of the IGSO satellites is thus about 40% (1.5 dB) larger than that of the MEO satellites. However, the roughly 4 dB higher free space loss of the IGSO satellites compared to the MEO satellites is responsible for a still lower received power on the ground.

3.3 Error Budget

The link budget model of Eq. 1 includes several possible error sources for the transmit power computation. As discussed in Sect. 2.1, some of these, such as the unmodeled atmospheric losses (< 0.1 dB) and polarization mismatch losses, can generally be neglected in the overall error budget. Dominating contributions result from uncertainties of the assumed receive antenna gain as well as the transmit antenna gain patterns.

In the Weilheim signal monitoring facility, the overall system gain is regularly calibrated using an extragalactic radio source and independent calibrations of the low-noise amplifiers using a signal generator. The total calibration uncertainty has been assessed in Thoelert et al. (2009) and amounts to less than 0.7 dB. This value also includes the impact of the high-gain antenna pointing accuracy, which has been verified to be better than 0.1°.

Concerning the uncertainty of the transmit antenna gain patterns, Wu (2002) reports differences of 0.25 dB for L1 and 0.35 dB for L2 between gain pattern measurements by two independent institutions. A similar uncertainty of ± 0.25 dB is provided for directivity measurements in Marquis (2016). Regarding the impact of the transmit antenna pointing accuracy, no detailed information is available, but peak gradients of 0.5–1 dB/deg may be inferred from the available gain patterns. At a representative GNSS satellite attitude control accuracy of better than 0.5° (Hegarty 2017), this corresponds to errors of 0.25–0.5 dB in EIRP measurements for a single epoch and boresight angle. Since the transmit powers are always derived from a full path of a GNSS satellite, a notable averaging of these individual errors occurs and a typical total error contribution of about 0.1 dB can be assumed.

Based on the error contributions discussed above, the total transmit power measurement accuracy is assumed to be at the level of 1 dB. However, a further uncertainty in the transmit power budget presented in Sect. 2.1 stems from the fact that only navigation signals in the upper and lower L-band have been taken into account in our work. These are not the only transmissions, however, given that a couple of other RF signals are used for payload and satellite operations on the GNSS satellites. Examples include

Table 3 Average transmit power of different types of GNSS satellites

System	Type	Group	SVN	Transmit power [W]
GPS	IIA		G022–G040	50
	IIR-A/B		G041, G043–G047, G051, G054, G056, G059–G061	60
	IIR-M		G048–G050, G052, G053, G055, G057, G058	145
	IIF		G062–G073	240
GLONASS	M	L1L/L2L	R735 since 2 Feb. 2016	20
		L1L/L2M	R715, R721, R733, R734, R736	25
		L1L/L2H	R719	40
		L1M/L2H	R716, R720	60
		L1H/L2M	R717, R730, R732	65
		L1H/L2H	R720, R731, R742–R745, R747, R851, R853, R854	85
		Default	Default value for all other GLONASS-M satellites	50
	K1		R801	135
			R802	105
	M+		R855	100
Galileo	IOV	n	E101–E104 until approximately 27 May 2014	160
		r	E101 and E102 (measured in Dec. 2015 and Oct. 2016)	135
		b	E103 (measured in Oct. 2016)	95
	FOC		E201–E214	265
BeiDou-2	MEO		C012–C015	130
	IGSO		C005, C007–C010, C017	185
QZSS	QZS-1		J001	244

All measured values are rounded to 5 W. The QZS-1 transmit power is taken from Kogure et al. (2017). *IOVn*: Galileo IOV satellites with nominal transmit power before July 2014; *IOVr*: Galileo IOV satellites with reduced transmit power after July 2014; *IOVb*: Galileo IOV satellites with status "all bands in temporary back-off' after July 2014

- Tracking, telemetry and command (TT&C) downlinks in S-band (e.g., GPS, Galileo, BDS) or C-Band (QZSS),
- Ultra high frequency (UHF) cross-links of the GPS nuclear detection system (Higbie and Blocker 1994),
- Search and rescue (SAR, Ilcev 2007) downlinks in L- and S-band,
- Radio determination satellite service (RDSS) of BeiDou-2 GEO satellites in C- and S-band (Yang et al. 2017).

Some of these transmissions, such as the SAR links, are known to be of low power (e.g., 5 W for Galileo, COSPAS-SARSAT 2013), and to operate only intermittently. Due to a lack of public information, as well as corresponding high-gain antenna measurements, we are currently unable to consider these signals in our analysis.

4 Modeling Antenna Thrust and Impact on Orbit Determination

According to Milani et al. (1987), the acceleration due to antenna thrust $\mathbf{a}_{\mathrm{AT}}$ can be expressed as

$$\mathbf{a}_{\mathrm{AT}} = \frac{P}{c \cdot m} \cdot \frac{\mathbf{x}_s}{|\mathbf{x}_s|} \tag{9}$$

with

P transmit power (Watt)
c vacuum speed of light
m satellite mass (kg)
$\mathbf{x}_s$ position vector of the satellite.

This expression assumes a narrow-beam, rotationally symmetric gain pattern and an antenna boresight directed toward the center of the Earth. As a result of these assumptions, no net acceleration perpendicular to the nadir direction arises and the resulting antenna thrust is always directed along the radius vector. As a simplification, Eq. 9 neglects the fact that only the projection of the radiated flux on the radial direction should be taken into account in the thrust computation. This is generally justified, since most of the energy is transmitted in the main lobe of the antenna. On average, over a 0 to 20° boresight angle range, the gain-weighted projection factor differs by about 2–3% from unity, which can safely be neglected in the present application. A more rigorous consideration of the power transmitted in sidelobes up to 90° boresight angle performed for GPS Block IIR/IIR-M satellites based on the gain patterns in Marquis and Reigh (2015) shows that the total antenna thrust is actually lower by 8%/4%

for L1 and 10%/5% for L2 than predicted by Eq. 9. In view of the absence of full gain pattern information for any of the other GNSS satellite types, we have, however, chosen not to apply this correction factor in our results.

At a given orbital period T, the radius r of the orbit as derived in a dynamical orbit determination changes by

$$\Delta r = -\frac{1}{3}\left(\frac{T}{2\pi}\right)^2 \cdot a_{AT} \tag{10}$$

when considering antenna thrust in the orbit model (Montenbruck et al. 2015b). That means that the radial change depends linearly on the transmit power and the inverse of the mass, and quadratically on the orbital period.

At a representative mass of 1000 kg and a transmit power of 100 W, the antenna thrust acceleration amounts to 0.3 nm/s^2, which in turn causes a change in the orbital radius by -5 mm for a 12-h orbit. For signals transmitted toward the center of the Earth, the acceleration caused by the antenna thrust is always directed in an outwards radial direction. This results in a decrease in the orbital radius compared to an orbit of identical period in the absence of antenna thrust.

4.1 Satellite Mass

As the magnitude of the antenna thrust is inversely proportional to the satellite mass (see Eq. 9), knowledge of the approximate mass is required for modeling of this effect. One has to distinguish between the dry mass, the launch mass (including the total amount of propellant), and the current in-orbit mass (including the amount of propellant for orbit and attitude maneuvers as well as end-of-life operations, i.e., disposal of the satellite into a graveyard orbit). For satellites that are directly injected into the target orbit by the launcher (e.g., GPS Block IIF, Galileo), in-orbit mass and launch mass differ only slightly. However, differences by a factor of up to two are present if the satellite is inserted into a transfer orbit by the launcher and reaches the final orbit with its own apogee kick motor (e.g., GPS Block IIR).

In-orbit mass values of historic, active, and selected future GNSS satellites are listed in Table 4. Reliable mass data are only publicly available for Galileo. The other values collated here are more or less rough estimates from different sources. Values for the in-orbit mass of the GPS and GLONASS satellites published in the literature differ by at most 6% which offers sufficient precision for the current work.

For BeiDou-2 IGSO satellites, much larger mass inconsistencies of several 100 kg can be found. Therefore, the mass of this satellite type is derived from the solar radiation pressure (SRP) force in satellite-Sun direction ($F_D = -16.9375 \times 10^{-5}$ N) obtained from ray-tracing given by Feng et al. (2014). Based on a mean value $D_0 = 122$ nm/s^2, of the SRP parameter estimated in BeiDou orbit determination by the authors of the present article, an approximate mass of 1400 kg can be inferred.

Table 4 In-orbit masses of different types of GNSS satellites. FOCe denotes the Galileo FOC satellites in eccentric orbit (E201 and E202)

System	Type	Mass (kg)	Reference
GPS	I	455	[a]
	II	843	[a]
	IIA	930	[a,b]
	IIR	1080	[c]
	IIR-M	1080	[c]
	IIF	1633	[d]
GLONASS	M	1415	[e,f]
	K1	995	[f]
	M+	$\geq$ 1415	[f]
	K1+	$\geq$ 995	[f]
	K2	1645	[e]
Galileo	IOV	695	[g]
	FOCe	660	[h]
	FOC	705–710	[h]
BDS-2	MEO	800	[i]
	IGSO	$\approx$ 1400	[j]
BDS-3	MEO	1014	[k]
QZSS	QZS-1	$\approx$ 2000	[l]

[a] Kramer (2002)
[b] https://ilrs.cddis.eosdis.nasa.gov/missions/satellite_missions/past_missions/gp35_general.html
[c] Hegarty (2017)
[d] http://www.boeing.com/space/global-positioning-system/#/technical-specifications
[e] Fatkulin et al. (2012)
[f] Revnivykh et al. (2017)
[g] European GNSS Service Center (2016)
[h] https://ilrs.cddis.eosdis.nasa.gov/missions/satellite_missions/current_missions/ga05_com.html
[i] https://directory.eoportal.org/web/eoportal/satellite-missions/c-missions/cnss
[j] derived from estimates of the direct solar radiation pressure
[k] http://spaceflight101.com/spacecraft/beidou-3/
[l] Montenbruck et al. (2017)

For QZS-1, only a launch mass of 4100 kg and a dry mass of 1800 kg are published in Inaba et al. (2009). Based on these values, Montenbruck et al. (2017) assumed a current in-orbit mass of 2000 kg. It has to be noted that Table 4 also provides mass values for spacecraft not covered by the high-gain antenna measurements discussed so far.

4.2 Impact on Orbit Determination

In order to study the impact of antenna thrust on GNSS orbit determination, global GNSS solutions have been computed with the NAPEOS software (Agueda and Zandbergen 2004). The tracking network of 150 stations is composed of

Table 5 Important modeling options for the precise orbit determination

Basic observable	Ionosphere-free linear combination of L1 and L2 for GPS/GLO/QZS E1 and E5a for GAL B1 and B2 for BDS
Observation sampling	300 s
Elevation cutoff angle	10°
Antenna model	igs14.atx, Rebischung et al. (2016b)
A priori SRP model	None for GPS/GLO/BDS Montenbruck et al. (2015b) for GAL Montenbruck et al. (2017) for QZS
Earth albedo	Agueda and Zandbergen (2004)
Antenna thrust	None/based on Tables 3 and 4

Table 6 Estimated parameters in the precise orbit determination

Parameter	Parameterization	Validity interval
Station coordinates	Offset	24 h
Receiver and satellite clocks	Offset	Epoch, 5-min sampling
Inter-system bias	Station-specific	24 h
Troposphere zenith delay	Piece-wise linear	2 h
Polar motion	Offset and drift	24 h
UT1	Drift	24 h
Satellite orbit	State vector	24 h
Solar radiation pressure	D_0, Y_0, B_0, B_C, B_S	24 h
Ambiguities	Fixed for GPS and GAL Float for GLO/BDS/QZS	Per arc

about 50 legacy IGS stations providing GPS and GLONASS observations and about 100 multi-GNSS stations providing observations of GPS and at least one of the new GNSSs. Table 5 lists important modeling options and Table 6 lists the estimated parameters. Ambiguities are fixed to integers with the Melbourne-Wübbena approach (Melbourne 1985; Wübbena 1985) for GPS and Galileo.

Daily solutions with and without considering antenna thrust have been computed for the time period December 2016 until May 2017 (336/2016 – 151/2017). In order to cover a significant amount of GPS Block IIA satellites including both spacecraft with a satellite laser ranging retroreflector (see Sect. 4.3), an additional analysis period from October 2012 to March 2013 (306/2012 – 120/2013) has been included. Mean radial orbit differences between solutions with and without antenna thrust are given in Table 7.

Due to their similar mass and transmit power, GPS Block IIA and IIR satellites experience both a radial shift of about 3 mm. GPS Block IIR-M and IIF satellites have a similar radial change of about 8 mm as the increased transmit power of the Block IIF satellites is accompanied by an increased mass. GLONASS-M satellites exhibit the smallest radial changes of 1–3 mm depending on their group affiliation. GLONASS-K1 and GLONASS-M+ show radial changes of 3 and 4 mm, respectively. Both satellite blocks are only covered by one spacecraft as the unhealthy GLONASS-K1 satellite R801 is not included in the analysis.

Due to their high transmit power and their low mass, the Galileo FOC satellites show the largest radial change of the MEO satellites. It amounts to 27 mm and is almost a factor of two larger than for the Galileo IOV satellites with reduced power (IOVr). The Galileo satellite with the status temporary back-off (E103) and the BeiDou-2 MEO satellites experience both a shift of 10 mm. The satellites in inclined geosynchronous orbit, namely BeiDou-2 IGSO and QZSS, have the largest radial change of 27 and 25 mm, respectively, mainly due to their large orbit height.

The orbit determination results for the mean radial orbit shift induced by the consideration of antenna thrust agree in general to better than 0.2 mm with predictions from the simplified analytical model (Eq. 10). On the other hand, orbit-periodic differences with a peak-to-peak amplitude of 15 mm for the eccentric FOCe satellite are not covered by that model and can only be evidenced in the more rigorous orbit determination process.

Table 7 Mean radial orbit differences obtained from 6 months of solutions with and without antenna thrust. FOCe denotes the Galileo FOC satellites in eccentric orbit (E201 and E202)

System	Type	Group	# sat	dR (mm)
GPS	IIA		9	− 2.8
	IIR-A/B		12	− 2.8
	IIR-M		7	− 7.0
	IIF		12	− 7.6
GLONASS	M	L1L/L2L	1	− 0.8
		L1L/L2M	5	− 1.0
		L1L/L2H	1	− 1.4
		L1M/L2H	2	− 2.0
		L1H/L2M	3	− 2.2
		L1H/L2H	10	− 2.9
	K1	R802	1	− 4.9
	M+		1	− 3.3
Galileo	IOV	r	2	− 13.9
		b	1	− 9.8
	FOCe		2	− 24.7
	FOC		12	− 27.0
BeiDou-2	MEO		3	− 9.8
	IGSO		6	− 27.4
QZSS	QZS-1		1	− 25.0

4.3 Orbit Validation with Satellite Laser Ranging

Satellite laser ranging (SLR) can be used for an independent validation of the radial component of GNSS satellite orbits. SLR normal points are provided by the International Laser Ranging Service (ILRS, Pearlman et al. 2002). Whereas all GLONASS, Galileo, BeiDou, and QZSS satellites are equipped with a laser retroreflector array (LRA), only two GPS Block IIA spacecraft can be tracked by SLR. For BeiDou-2, only three of the MEO and IGSO spacecraft are tracked by the ILRS on a regular basis. Detailed analysis of SLR measurements to GPS and GLONASS is given in Sosnica et al. (2015).

Station coordinates are fixed to SLRF2014,[2] an elevation cutoff of 10° is used, and the tropospheric model of Mendes and Pavlis (2004) is applied. SLR residuals between the orbit determined by microwave observations and the range observed by SLR are computed. In the absence of systematic errors, the bias of these residuals is expected to be zero. Primarily due to GNSS orbit modeling deficiencies, biases of − 20 to + 40 mm are present for the GPS, GLONASS, and Galileo satellites, whereas the biases of BeiDou and QZSS can reach up to 15 cm.

[2] ftp://ftp.cddis.eosdis.nasa.gov/slr/products/resource.

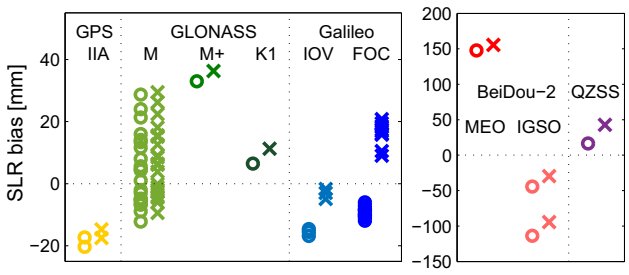

Fig. 11 Satellite laser ranging residual biases for orbit solutions without antenna thrust (indicated by *circles*) and orbit solutions considering antenna thrust (indicated by *crosses*)

SLR biases for orbit solutions with and without applying antenna thrust are shown in Fig. 11. Whereas the absolute SLR biases get smaller for GPS Block IIA, Galileo IOV, and BeiDou-2 IGSO satellites, they increase for GLONASS-M+ and -K1, Galileo FOC satellites in nominal orbit, BeiDou-2 MEO and QZSS if antenna thrust is applied. For GLONASS-M, the absolute SLR bias gets larger for 13 out of 22 satellites.

Overall, consideration of antenna thrust does not appear to improve the leveling of GNSS satellite orbits determined from radiometric tracking. However, this is not necessarily caused by deficiencies in the antenna thrust model or power levels retrieved in the present analysis, which are believed to be accurate to typically 25% or better. The finding rather indicates additional modeling errors of unknown origin. As a likely candidate, the simplifying nature of present solar and Earth radiation pressure models can be identified. By way of example, the proper consideration of shading effects for selected structural elements of GIOVE-B (Steigenberger et al. 2015) has been shown to induce radial offsets in the resulting orbits of up to 10 cm. With such effects in mind, the consideration of antenna thrust will only pay off if other non-gravitational forces are modeled with an accuracy level of 1–10 mm in terms of the radial orbit component.

5 Summary and Outlook

Modeling antenna thrust requires information about the total transmit power of a GNSS satellite, which is usually not publicly available. Therefore, the total transmit power of selected GNSS satellites has been measured with a 30-m dish antenna. Transmit power values between 20 W for one particular GLONASS-M spacecraft and 265 W for Galileo FOC have been obtained. Aside from remaining uncertainties in the high-gain antenna calibration, major limitations result from an incomplete knowledge of transmit antenna gain patterns for GPS Block IIF, BeiDou-2, and in particular GLONASS. Overall, the presented transmit power values exhibit presumed uncertainty at the level of 1 dB or equivalently 25%.

The orbital radius of GNSS satellites changes by 1–27 mm depending on transmit power, mass, and orbital period if antenna thrust is considered in the precise orbit determination. Validation of these orbits with satellite laser ranging does not show a clear improvement compared to orbits without considering antenna thrust. However, this is likely related to remaining modeling deficiencies of solar and Earth radiation pressure, which are larger than the impact of antenna thrust.

Prior to the practical use of the new antenna thrust values in the IGS product generation, a readjustment of the satellite antenna z-offsets might be necessary due to the high correlations of these parameters with the orbital scale. Reprocessing efforts as conducted by the IGS in support of new releases of the International Terrestrial Reference Frame (ITRF) will also require transmit power values for old generations of satellites such as GPS Block I and the first-generation GLONASS satellites that are not covered by the present study. Since it is no longer possible to measure such values with the current facilities, a public release of corresponding information by the manufacturers and providers of these constellations is encouraged.

The current study is also incomplete concerning new generations of GNSS satellites that are expected to be launched in the near future or are already in orbit. The first GPS Block III is expected to be launched in 2018 and will provide the new L1C civil signal (Betz et al. 2007). GLONASS-K1+ satellites will transmit additional CDMA signals on L2, GLONASS-K2 satellites on L1 and L2 (Revnivykh et al. 2017). Five BeiDou-3 satellites have been launched in 2015/2016 transmitting several new signals in addition to signals backwards-compatible to BeiDou-2 (Xiao et al. 2015). The second QZSS satellite QZS-2 was already launched in June 2017 and is expected to transmit an additional protected signal on E6 similar to the Galileo Public Regulated Service (PRS). For none of these satellites, transmit antenna gain patterns are publicly available up to now. Availability of these gain patterns is a prerequisite for future analysis of the corresponding transmit power and a proper modeling of antenna thrust for these new satellites.

Acknowledgements We thank the European Space Agency for granting access to the NAPEOS software version 3.3.1, the International GNSS Service (IGS) and the International Laser Ranging Service (ILRS) for providing GNSS and SLR observation data.

References

Agueda A, Zandbergen R (2004) NAPEOS mathematical models and algorithms. Technical report, NAPEOS-MM-01, iss. 3.0, 04/06/2004, ESA/ESOC, Darmstadt

Ajioka J, Harry H (1970) Shaped beam antenna for Earth coverage from a stabilized satellite. IEEE Trans Antenna Propag 18(3):323–327. https://doi.org/10.1109/TAP.1970.1139681

Baars J, Genzel R, Pauliny-Thoth I, Witzel W (1977) The absolute spectrum of Cas A: an accurate flux density scale and a set of second calibrators. Astron Astrophys 61(1):99–106

Barker BC, Betz JW, Clark JE, Correia JT, Gillis JT, Lazar S, Rehborn KA, Straton JR (2000) Overview of the GPS M code signal. In: ION NTM 2000. Anaheim, pp 542–549

Betz J, Blanco M, Cahn C, Dafesh P, Hegarty C, Hudnut K, Kasemsri V, Keegan R, Kovach K, Lenahan L, Ma H, Rushanan J, Sklar D, Stansell T, Wang C, Yi S (2007) Enhancing the future of civil GPS: overview of the L1C signal. Inside GNSS 2(3):42–49

Chang X, Mei X, Yang H (2015) Space service volume performance of BDS. In: 10th Meeting of the International Committee on Global Navigation Satellite Systems (ICG-10)

COSPAS-SARSAT (2013) Description of the 406 MHz payloads used in the COSPAS-SARSAT MEOSAR system. Technical report, http://vnmcc.vishipel.vn/images/uploads/attach/T016.PDF

Czopek F, Shollenberger S (1993) Description and performance of the GPS Block I and II L-band antenna and link budget. In: ION GPS 1993. Salt Lake City, pp 37–43

Dow JM, Neilan RE, Rizos C (2009) The International GNSS Service in a changing landscape of Global Navigation Satellite Systems. J Geod 83(3–4):191–198. https://doi.org/10.1007/s00190-008-0300-3

Eanes RJ, Nerem RS, Abusali P, Bamford W, Key K, Ries JC, Schutz BE (1999) GLONASS orbit determination at the Center for Space Research. In: Slater J, Noll C, Gowey K (eds) International GLONASS Experiment IGEX-98 Workshop Proceedings, IGS. Jet Propulsion Laboratory, pp 209–217

Edgar C, Price J, Reigh D (1998) GPS Block IIA and IIR received signal power measurements. In: ION NTM 1998. Long Beach, pp 401–411

Edgar C, Goldstein DB, Bentley P (2002) Current constellation GPS satellite ground received signal power measurements. In: ION NTM 2002. San Diego, pp 948–954

European GNSS Service Center (2016) Galileo IOV satellite metadata. European Global Navigation Satellite Systems Agency, https://www.gsc-europa.eu/support-to-developers/galileo-iov-satellite-metadata

Falcone M (2016) Galileo system status. In: ION GNSS+ 2016. Portland, pp 2410–2430

Fatkulin R, Kossenko V, Storozhev S, Zvonar V, Chebotarev V (2012) GLONASS space segment: satellite constellation, Glonass-M and Glonass-K spacecraft main features. ION GNSS 2012:3912–3930

Feng W, Guo X, Qiu H, Zhang J, Dong K (2014) A study of analytical solar radiation pressure modeling for BeiDou navigation satellites based on raytracing method. In: Sun J, Jiao W, Wu H, Lu M (eds) China Satellite Navigation Conference (CSNC) 2014 Proceedings: volume II, Lecture Notes in Electrical Engineering. Springer, Berlin, pp 425–435. https://doi.org/10.1007/978-3-642-54743-0_35

Fisher SC, Ghasemi K (1999) GPS IIF—the next generation. Proc IEEE 87(1):24–47. https://doi.org/10.1109/5.736340

Ghasemi A, Abedi A, Ghasemi F (2012) Basic principles in radio wave propagation. In: Propagation engineering in wireless communications, chap 2. Springer, New York, pp 23–55. https://doi.org/10.1007/978-1-4614-1077-5_2

Hauschild A, Montenbruck O, Thoelert S, Erker S, Meurer M, Ashjaee J (2012) A multi-technique approach for characterizing the SVN49 signal anomaly, part 1: receiver tracking and IQ constellation. GPS Solut 16(1):19–28. https://doi.org/10.1007/s10291-011-0203-2

Hegarty C (2017) The Global Positioning System (GPS). In: Teunissen P, Montenbruck O (eds) Springer Handbook of Global Navigation Satellite Systems, chap 7. Springer, Berlin, pp 197–218. https://doi.org/10.1007/978-3-319-42928-1_7

Higbie P, Blocker N (1994) Detecting nuclear detonations with GPS. GPS World 5(2):48–50

ICD-GPS-200C (2000) Interface conrol document ICD-GPS-200: Navstar GPS space segment/navigation user segment interfaces. Technical report, ARINC Research Corporation, http://www.gps.gov/technical/icwg/ICD-GPS-200C.pdf

IGS (2011) Calculated and estimated GPS transmit power levels. http://acc.igs.org/orbits/thrust-power.txt

Ilcev DS (2007) Cospas-Sarsat LEO and GEO: satellite distress and safety systems (SDSS). Int J Satell Commun Netw 25(6):559–573

Inaba N, Matsumoto A, Hase H, Kogure S, Sawabe M, Terada K (2009) Design concept of Quasi Zenith Satellite System. Acta Astronaut 65(7–8):1068–1075. https://doi.org/10.1016/j.actaastro.2009.03.068

Irsigler M, Hein GW, Schmitz-Peiffer A (2004) Use of C-band frequencies for satellite navigation: benefits and drawbacks. GPS Solut 8(3):119–139. https://doi.org/10.1007/s10291-004-0098-2

IS-GPS-200E (2010) Interface specification IS-GPS-200: Navstar GPS space segment/navigation user segment interfaces. Technical report, Global Positioning System Wing (GPSW) Systems Engineering and Integration. http://www.gps.gov/technical/icwg/IS-GPS-200E.pdf

IS-GPS-200H (2014) Interface specification IS-GPS-200: Navstar GPS space segment/navigation user segment interfaces. Technical report, Global Positioning Systems Directorate Systems Engineering and Integration. http://www.gps.gov/technical/icwg/IS-GPS-200H.pdf

IS-GPS-705A (2010) Navstar GPS space segment/user segment L5 interfaces. Technical report, Global Positioning System Wing (GPSW) Systems Engineering and Integration. http://www.gps.gov/technical/icwg/IS-GPS-705A.pdf

IS-GPS-800A (2010) Navstar GPS space segment/user segment L1C interface. Technical report, Global Positioning System Wing (GPSW) Systems Engineering and Integration. http://www.gps.gov/technical/icwg/IS-GPS-800A.pdf

IS-QZSS-L1S-001 (2017) Quasi-Zenith Satellite System Interface Specification Sub-meter Level Augmentation Service. Technical report, Cabinet Office. http://qzss.go.jp/en/technical/download/pdf/ps-is-qzss/is-qzss-pnt-001.pdf

ITU-R (2005) Specific attenuation model for rain for use in prediction methods. Recommendation ITU-R P.838-3, Radiocommunication Sector of International Telecommunication Union (ITU-R)

ITU-R (2013a) Attenuation by atmospheric gases. Recommendation ITU-R P.676-10, Radiocommunication Sector of International Telecommunication Union (ITU-R)

ITU-R (2013b) Attenuation due to clouds and fog. Recommendation ITU-R P.840-6, Radiocommunication Sector of International Telecommunication Union (ITU-R)

ITU-R (2013c) Reference standard atmospheres. Recommendation ITU-R P.676-10, Radiocommunication Sector of International Telecommunication Union (ITU-R)

Kogure S, Ganeshan AS, Montenbruck O (2017) Regional systems. In: Teunissen P, Montenbruck O (eds) Springer Handbook of Global Navigation Satellite Systems, chap 11. Springer, Berlin. pp 305–337. https://doi.org/10.1007/978-3-319-42928-1_11

Kramer HJ (2002) Observation of the earth and its environment: survey of missions and sensors, 4th edn. Springer, Berlin. https://doi.org/10.1007/978-3-642-56294-5

Marquis W (2014) The GPS Block IIR/IIR-M antenna panel pattern: Appendix B - SV-specific patterns, data. Lockheed Martin Space Systems Company. http://www.lockheedmartin.com/content/dam/lockheed/data/space/photo/gps/gpspubs/Appendix

Marquis W (2015) The GPS Block IIR/IIR-M antenna panel pattern. Lockheed Martin Space Systems Company. http://www.lockheedmartin.com/content/dam/lockheed/data/space/documents/gps/GPS-Block-IIR-and-IIR-M-Antenna-Panel-Pattern-Marquis-Aug2015-revised.pdf

Marquis W (2016) The GPS Block IIR antenna panel pattern and its use on-orbit. In: ION GNSS+ 2016. Portland, pp 2896–2909

Marquis WA, Reigh DL (2015) The GPS Block IIR and IIR-M broadcast L-band antenna panel: its pattern and performance. Navigation 62(4):329–347. https://doi.org/10.1002/navi.123

Melbourne WG (1985) The case for ranging in GPS based geodetic systems. In: Goad C (ed) Proceedings of the First International Symposium on Precise Positioning with the Global Positioning System, U.S. Department of Commerce, Rockville, pp 373–386

Mendes VB, Pavlis EC (2004) High-accuracy zenith delay prediction at optical wavelengths. Geophys Res Lett 31:L14602. https://doi.org/10.1029/2004GL020308

Milani A, Nobili AM, Farinella P (1987) Non-gravivational perturbations and satellite geodesy. Adam Hilger, Bristol

Mölders N, Kramm G (2014) Lectures in meteorology. Springer, Berlin

Montenbruck O, Schmid R, Mercier F, Steigenberger P, Noll C, Fatkulin R, Kogure S, Ganeshan A (2015) GNSS satellite geometry and attitude models. Adv Space Res 56(6):1015–1029. https://doi.org/10.1016/j.asr.2015.06.019

Montenbruck O, Steigenberger P, Hugentobler U (2015b) Enhanced solar radiation pressure modeling for Galileo satellites. J Geod 89(3):283–297. https://doi.org/10.1007/s00190-014-0774-0

Montenbruck O, Steigenberger P, Darugna F (2017) Semi-analytical solar radiation pressure modeling for QZS-1 orbit-normal and yaw-steering attitude. Adv Space Res 59(8):2088–2100. https://doi.org/10.1016/j.asr.2017.01.036

Montesano A, Montesano C, Caballero R, Naranjo M, Monjas F, Cuesta LE, Zorrilla P, Martínez L (2007) Galileo system navigation antenna for global positioning. In: Proceedings of EuCAP 2007

Noda H, Kogure S, Kishimoto M, Soga H, Moriguchi T, Furubayashi T (2010) Development of the Quasi-Zenith Satellite System and high-accuracy positioning experiment system flight model. NEC Tech J 5(3):93–97

NovAtel Inc (2006) GPS-704X antenna design and performance. Technical report. http://www.novatel.com/assets/Documents/Papers/GPS-704xWhitePaper.pdf

Pearlman M, Degnan J, Bosworth J (2002) The International Laser Ranging Service. Adv Space Res 30(2):125–143. https://doi.org/10.1016/S0273-1177(02)00277-6

Rebeyrol E, Macabiau C, Ries L, Bousquet M, Bouchere ML (2006) Interplex modulation for navigation systems at the L1 band. In: ION NTM 2006. Monterey, pp 100–111

Rebischung P, Altamimi Z, Ray J, Garayt B (2016a) The IGS contribution to ITRF2014. J Geod 90(7):611–630. https://doi.org/10.1007/s00190-016-0897-6

Rebischung P, Schmid R, Herring T (2016b) Upcoming switch to IGS14/igs14.atx. IGSMAIL-7399. https://igscb.jpl.nasa.gov/pipermail/igsmail/2016/008589.html

Revnivykh S, Bolkunov A, Serdyukov A, Montenbruck O (2017) GLONASS. In: Teunissen P, Montenbruck O (eds) Springer Handbook of Global Navigation Satellite Systems, chap 8. Springer, Berlin, pp 219–245. https://doi.org/10.1007/978-3-319-42928-1_8

Rodriguez-Solano C, Hugentobler U, Steigenberger P (2012) Impact of albedo radiation on GPS satellites. In: Geodesy for Planet Earth, Springer, International Association of Geodesy Symposia 136:113–119. https://doi.org/10.1007/978-3-642-20338-1_14

Schrank H (1983) Antenna designer's notebook: polarization mismatch loss. IEEE Antennas Propag Soc Newslett 25(4):28–29. https://doi.org/10.1109/MAP.1983.27697

Seybold JS (2005) Introduction to HF propagation. Wiley, Hoboken

Sosnica K, Thaller D, Dach R, Steigenberger P, Beutler G, Arnold D, Jäggi A (2015) Satellite laser ranging to GPS and GLONASS. J Geod 89(7):725–743. https://doi.org/10.1007/s00190-015-0810-8

Spence R (2010) Reference assumptions for GPS/Galileo compatibility analyses. NASA, Washington

Spilker Jr JJ (1996) Tropospheric effects on GPS. In: Parkinson BW, Spilker Jr JJ (eds) Global Positioning System: theory and applications volume I, Progress in Astronautics and Aeronautics, chap 13, Vol 163, American Institute of Aeronautics and Astronautics, pp 517–546

Steigenberger P, Montenbruck O (2016) Galileo status: orbits, clocks, and positioning. GPS Solut 21(2):319–331. https://doi.org/10.1007/s10291-016-0566-5

Steigenberger P, Montenbruck O, Hugentobler U (2015) GIOVE-B solar radiation pressure modeling for precise orbit determination. Adv Space Res 55(5):1422–1431. https://doi.org/10.1016/j.asr.2014.12.009

Steigenberger P, Hauschild A, Langley R (2017) US Air Force puts more power into GPS Block IIR-M C/A-code. GPS World 28(4):8–9

Thoelert S, Erker S, Meurer M (2009) GNSS signal verification with a high gain antenna—calibration strategies and high quality signal assessment. In: ION ITM 2009. Portland, pp 2896–2909

Thoelert S, Furthner J, Meurer M (2012) New birds in the sky—signal in space (SIS) analysis of new GNSS satellites. In: ION GNSS 2012. Nashville, pp 3613–3619

Thoelert S, Meurer M, Erker S, Montenbruck O, Hauschild A, Fenton P (2012b) A multi-technique approach for characterizing the SVN49 signal anomaly, part 2: chip shape analysis. GPS Solut 16(1):29–39. https://doi.org/10.1007/s10291-011-0204-1

Thoelert S, Furthner J, Meurer M (2013) GNSS survey—signal quality assessment of the latest GNSS satellites. In: ION ITM 2013. San Diego, pp 608–615

Thoelert S, Montenbruck O, Meurer M (2014) IRNSS-1A: signal and clock characterization of the Indian regional navigation system. GPS Solut 18(1):147–152. https://doi.org/10.1007/s10291-013-0351-7

Valle P, Netti A, Zolesi M, Mizzoni R, Bandinelli M, Guidi R (2006) Efficient dual-band planar array suitable to GALILEO. In: Proceedings First European Conference on Antennas and Propagation (EuCAP 2006). https://doi.org/10.1109/EUCAP.2006.4584868

Visser HJ (2012) Antenna theory and applications. Wiley, Hoboken

Wu A (2002) Predictions and field measurements of the GPS Block IIR L1 and L2 ground powers. In: ION NTM 2002. San Diego, pp 931–938

Wübbena G (1985) Software developments for geodetic positioning with GPS using TI-4100 code and carrier measurements. In: Goad C (ed) Proceedings of the First International Symposium on Precise Positioning with the Global Positioning System, U.S. Department of Commerce, Rockville, pp 403–412

Xiao W, Liu W, Sun G (2015) Modernization milestone: BeiDou M2-S initial signal analysis. GPS Solut 20(1):125–133. https://doi.org/10.1007/s10291-015-0496-7

Yang Y, Tang J, Montenbruck O (2017) Chinese navigation satellite systems. In: Teunissen P, Montenbruck O (eds) Springer Handbook of Global Navigation Satellite Systems, chap 10. Springer, Berlin, pp 273–304. https://doi.org/10.1007/978-3-319-42928-1_10

Ziebart M, Edwards S, Adhya S, Sibthrope A, Arrowsmith P, Cross P (2004) High precision GPS IIR orbit prediction using analytical non-conservative force models. In: ION GNSS 2004. Long Beach, pp 1764–1770

Ziebart M, Sibthrope A, Cross P, Bar-Sever Y, Haines B (2007) Cracking the GPS-SLR orbit anomaly. In: ION GNSS 2007. Fort Worth, pp 2033–2038